NPP-21/TPR is required for developmental control of spindle checkpoint strength in *C. elegans*

Natalie Gallagher[#], Shevelle Brown[#], Valentin Duprat[#], Simone Köhler*[§], Abby F. Dernburg*, and Needhi Bhalla[#]

[#]Department of Molecular, Cell and Developmental Biology, University of California, Santa Cruz, Santa Cruz, CA 95064

*Department of Molecular and Cell Biology, University of California, Berkeley, Berkeley, CA 94720

[§]Current address: Cell Biology and Biophysics Unit, European Molecular Biology Laboratory, 69117 Heidelberg, Germany

[1] corresponding author: nbhalla@ucsc.edu

Department of Molecular, Cell and Developmental Biology

225 Sinsheimer Labs

University of California, Santa Cruz

Santa Cruz, CA 95064

phone: (831) 459-1319

fax: (831) 459-3139

Abstract

The spindle checkpoint ensures accurate chromosome segregation by monitoring whether chromosomes, via kinetochores, are properly attached to the mitotic or meiotic spindle. If chromosomes are unattached, the checkpoint delays the cell cycle to facilitate error correction. In *C. elegans* early embryos, activation of the spindle checkpoint produces a longer mitotic delay in cells that will become germline tissue than in cells that will become somatic tissue, suggesting developmental regulation. We show that the conserved nucleoporin and spindle matrix component, NPP-21/TPR, is required for the stronger spindle checkpoint in germline cells. A strain expressing AID-3xFLAG-NPP-21 and the Arabidopsis TIR1 gene cannot support the stronger checkpoint in germline cells. When AID-3xFLAG-NPP-21 is acutely degraded, the checkpoint in germline cells is further compromised while somatic cells are unaffected. A checkpoint-proficient NPP-21-GFP transgene localizes to a spindle-like structure during mitosis and is enriched in germline cells, consistent with a cell-fate specific function for this protein. Finally, NPP-21 controls spindle checkpoint strength in germline cells by two, potentially linked, control points: concentrating PCH-2 around mitotic chromosomes and promoting the localization of the checkpoint effector, Mad2, to unattached kinetochores. These experiments demonstrate a developmental role for NPP-21, and the spindle matrix, in controlling spindle checkpoint strength in immortal germline cells in *C. elegans*.

Introduction

The spindle checkpoint is a cell cycle surveillance mechanism that ensures that chromosomes are attached to the mitotic or meiotic spindle to guarantee accurate chromosome segregation and prevent aneuploidy. When chromosomes are unattached, a soluble, molecular signal halts or delays the cell cycle to allow for the defect to be corrected. Defects in spindle checkpoint components are associated with cancer progression (Kops et al., 2005; Matthews et al., 2022) and infertility (Baker et al., 2004; Huang et al., 2023; Zhang et al., 2020), highlighting their importance to human health.

The spindle checkpoint initiates from unattached kinetochores, the specialized structures that assemble on chromosomes' centromeres to mediate microtubule attachment and proper segregation (Lara-Gonzalez et al., 2021). A complex of the conserved checkpoint factors, Mad1 and Mad2, binds unattached kinetochores. Mad2 adopts two functionally distinct conformations: an open, inactive form and a closed, active form. Mad2's conversion from inactive to active occurs when Mad2 binds a specific motif, called the closure motif, in binding partners. Mad2 binding partners, such as Mad1 and Cdc20, each have closure motifs and thus, catalyze the conversion of Mad2 from inactive to active. Once bound to unattached kinetochores, the Mad1/Mad2 complex recruits additional inactive Mad2 so that it can bind Cdc20, adopting the active conformation and forming the Mitotic Checkpoint Complex, or MCC. The MCC sequesters Cdc20, a factor required to promote anaphase, to inhibit the cell cycle and allow time for error correction (Lara-Gonzalez et al., 2021). The evolutionarily ancient ATP-ase PCH-2/TRIP13 plays a conserved role promoting spindle checkpoint function by ensuring the availability of open, inactive Mad2 (Ma and Poon, 2016; Ma and Poon, 2018; Nelson et al., 2015)

68 Despite the important role of the spindle checkpoint in preventing aneuploidy, the mitotic delay
69 or arrest installed by the spindle checkpoint can be highly variable. The variability of the cell
70 cycle delay is called spindle checkpoint strength and depends on the number of unattached
71 kinetochores, cell volume, and cell fate (Collin et al., 2013; Galli and Morgan, 2016; Gerhold et
72 al., 2018; Kyogoku and Kitajima, 2017). For example, during early embryogenesis in *C. elegans*,
73 cells that are destined to become germline tissue have a stronger checkpoint than their somatic
74 counterparts, independent of their smaller size (Galli and Morgan, 2016; Gerhold et al., 2018),
75 demonstrating developmental differences in checkpoint strength. We have shown that the
76 stronger checkpoint in germline cells depends on the asymmetric enrichment of the spindle
77 checkpoint factor, PCH-2/TRIP13 (Defachelles et al., 2020), likely through PCH-2/TRIP13's
78 ability to ensure more open, inactive Mad2 for increased MCC production.
79
80 We wanted to identify additional factors that might also contribute to the stronger checkpoint in
81 germline cells of the early embryo. We noticed that after nuclear envelope breakdown, PCH-2-
82 GFP and other checkpoint components, such as GFP-Mad1 and GFP-Mad2, formed a "cloud"
83 around mitotic chromosomes (Defachelles et al., 2020; Essex et al., 2009). This "cloud"
84 sometimes resembled a controversial mitotic structure called the spindle matrix (Zheng, 2010),
85 especially in germline cells. The spindle matrix has been observed in both *Drosophila* and
86 human somatic cells, but both its composition and essential function have been unclear. Some
87 spindle matrix components interact with spindle checkpoint components (Lince-Faria et al.,
88 2009; Schweizer et al., 2013), making them attractive candidates to potentially regulate spindle
89 checkpoint strength during development.
90
91 NPP-21/TPR is the *C. elegans* ortholog of the *Drosophila* spindle matrix protein, Megator, and
92 the human TPR. In *C. elegans*, NPP-21/TPR has been primarily characterized as a nucleoporin,
93 a member of a family of proteins which assemble the nuclear pore and allow for molecular

transport between the cytoplasm and nucleus (Cohen-Fix and Askjaer, 2017). NPP-21/TPR forms the nucleoplasmic face or basket of the pore (Cohen-Fix and Askjaer, 2017). In *Drosophila*, Megator is a nucleoporin but also localizes to the area occupied by the miotic spindle (Qi et al., 2004) and supports activation of the spindle checkpoint by ensuring robust recruitment of Mad2 to unattached kinetochores (Lince-Faria et al., 2009). We hypothesized that NPP-21 may play a similar role during development in *C. elegans* and that this role might be particularly relevant in germline cells during early embryogenesis.

Here, we show that NPP-21/TPR, in its capacity as a spindle matrix component, is required for developmental control of spindle checkpoint strength in *C. elegans*. A strain carrying both a transgene of *npp-21*, *AID-3xFLAG::npp-21*, and the Arabidopsis TIR1 gene is functional for checkpoint activation in somatic cells of the early embryo but cannot support the stronger checkpoint in germline cells, suggesting that the stronger checkpoint in these cells is sensitive to subtle changes in NPP-21 protein levels. When the tagged protein is acutely degraded, checkpoint strength is further compromised in germline cells but has no effect on somatic cells. Consistent with this cell-fate specific function, NPP-21-GFP consistently forms a structure that resembles the spindle matrix during mitosis and is asymmetrically enriched in germline cells, compared to somatic cells. Finally, NPP-21 ensures a stronger checkpoint in P_1 cells by concentrating PCH-2 around mitotic chromosomes and promoting the robust recruitment of Mad2 to unattached kinetochores.

Results and Discussion

NPP-21 is required for the stronger spindle checkpoint in germline, P_1 cells

119 NPP-21 is an essential gene. Therefore, to determine whether NPP-21 plays a role in the
120 spindle checkpoint in early developing embryos, we exploited the auxin-inducible degron system
121 (AID) to acutely degrade NPP-21 in oocytes and early embryos. We generated a version of
122 NPP-21 tagged at its N-terminus with the AID and a 3xFLAG tag (*AID-3xFLAG::npp-21*, also
123 referred to as *AID::npp-21*) in a strain that expresses the Arabidopsis TIR1 gene under a
124 germline promoter (*Pgld-1::TIR1-mRuby)* (Zhang et al., 2015). TIR1 is necessary to induce
125 rapid degradation of tagged proteins upon exposure to auxin. This tagged version of NPP-21, at
126 least in the presence of the TIR1 gene, mildly affects embryonic viability and meiotic
127 chromosome segregation, as *AID::npp-21* worms grown on ethanol produce inviable embryos
128 and males at a higher frequency than control worms exposed to either ethanol or auxin (Table
129 1). Since hermaphrodites are XX and males are XO, an increase in the number of male self-
130 progeny is indicative of defects in meiotic chromosome segregation. When *AID::npp-21* worms
131 were exposed to auxin, very few viable progeny were produced and among the viable progeny,
132 there was a significant increase in male self-progeny (Table 1). Thus, the *AID::npp-21* transgene
133 is mostly functional, with some slight defects in embryonic viability and meiotic chromosome
134 segregation, which may be the product of the tag and/or inappropriate TIR1 activity. By contrast,
135 auxin-induced depletion of *AID::npp-21* results in very high embryonic lethality and severe
136 defects in meiotic chromosome segregation, consistent with its essential role.
137
138 We tested whether we could reliably and rapidly degrade AID-3xFLAG-NPP-21. We performed
139 this experiment in the most proximal oocytes undergoing cellularization (-1 oocyte). Upon
140 fertilization, these oocytes complete meiosis and enter mitosis to begin embryonic development
141 within an hour (Robertson and Lin, 2013). We exposed young adult hermaphrodites worms
142 undergoing oogenesis to auxin for one hour and performed indirect immunofluorescence
143 against the FLAG tag to visualize NPP-21. In worms exposed to ethanol, we observed staining
144 surrounding the chromosomes in the most proximal oocytes, consistent with the protein being a

145 member of the nuclear pore complex in the nuclear envelope (Figure 1A). After one hour of
146 treatment, we could no longer detect AID-3xFLAG-NPP-21 at the nuclear periphery (Figure 1A),
147 indicating that we can reliably and rapidly degrade NPP-21 in oocytes that are about to be
148 fertilized and develop into embryos.
149
150 Having established this protocol, we used it to test whether degradation of NPP-21 affected
151 normal mitotic timing and spindle checkpoint function in early embryos, specifically two cell
152 embryos which have already initiated the process of cell differentiation into soma (AB cells) and
153 germline (P_1 cells) tissue (Figure 1B). We analyze mitotic timing by calculating the time between
154 nuclear envelope breakdown (NEBD) and the onset of cortical contractility (OCC) in embryos
155 that have an mCherry tagged histone, mCherry-H2B, and the plasma membrane marker, GFP-
156 PH (Essex et al., 2009). NEBD is visualized as the diffusion of soluble mCherry-H2B signal from
157 the nucleus and OCC is detected when the plasma membrane changes conformation from
158 circular to rectangular. We performed this experiment in both AB and P_1 cells since these two
159 different cells vary in both cell fate and spindle checkpoint strength (Figure 1B). P_1 cells have a
160 stronger checkpoint than their somatic counterparts and this is dependent on conserved factors
161 required for its developmental fate, independent of its smaller size (Galli and Morgan, 2016;
162 Gerhold et al., 2018). When transgenic *AID::npp-21* worms were exposed to ethanol or auxin,
163 we did not detect any difference in mitotic timing between ethanol-treated or auxin-treated
164 worms, or with control worms treated with ethanol, in either AB or P_1 cells, indicating that NPP-
165 21 is not required for unperturbed mitosis in either cell type (Figures 1C and D).
166
167 Next, we activated the spindle checkpoint in *AID::npp-21* AB cells by performing RNA
168 interference (RNAi) against *zyg-1*, a conserved cell cycle kinase required for centrosome
169 duplication (O'Connell et al., 2001). In the absence of *zyg-1*, two cell embryos only have one
170 centrosome and generate a monopolar spindle, producing unattached kinetochores and spindle

171 checkpoint activation (Essex et al., 2009). In AB cells of *zyg-1*^{RNAi} embryos, we observed a slight
172 decrease in mitotic timing in transgenic *AID::npp-21* worms on ethanol or auxin (Figure 1C),
173 when compared to control embryos on ethanol. This difference was not statistically significant,
174 indicating that NPP-21 might play a role in promoting a strong spindle checkpoint in AB cells but
175 is not required for the checkpoint in these cells. In contrast, when we activated the spindle
176 checkpoint in P_1 cells in *AID::npp-21* worms exposed to ethanol, these cells showed similar
177 mitotic timing as AB cells treated with *zyg-1* RNAi (Figures 1C and D) and a weaker checkpoint
178 than control worms (Figure 1D). These data indicate that either the transgenic *AID::npp-21* is
179 not fully functional for spindle checkpoint function in P_1 cells or that the presence of TIR1, even
180 in the absence of auxin, affects protein function. More importantly, these data suggest a role for
181 NPP-21 in spindle checkpoint strength in this specific cell type. When *AID::npp-21* worms are
182 exposed to auxin for more than one hour, we detected a further weakening of the spindle
183 checkpoint (Figure 1D), indicating that NPP-21 is required for a robust spindle checkpoint
184 specifically in P_1 cells.
185
186 **NPP-21-GFP adopts a structure similar to the spindle matrix and is enriched in P_1 cells**
187
188 Given this cell fate-specific difference in the requirement for NPP-21 function in the spindle
189 checkpoint, we localized NPP-21-GFP in AB and P_1 cells in two cell embryos (Thomas et al.,
190 2023). First, we verified that *npp-21::gfp* worms were competent for checkpoint activation in AB
191 and P_1 cells. Because the presence of NPP-21-GFP prevented us from using GFP-PH to
192 monitor OCC, we measured mitotic timing using mCherry-H2B from NEBD to decondensation of
193 mitotic chromosomes (DECON) (Essex et al., 2009). Both AB and P_1 cells in embryos
194 expressing NPP-21-GFP activated the spindle checkpoint and P_1 cells displayed a stronger
195 checkpoint than AB cells, similar to control worms (Figure 2A), verifying that NPP-21-GFP is
196 fully functional for checkpoint activation. Next, we localized NPP-21-GFP and observed a

197 striking difference in its localization in AB and P_1 cells. In 75% of two-cell embryos (6/8), NPP-
198 21-GFP remained in a cloud around mitotic chromosomes 120 seconds after NEBD, a timepoint
199 that corresponds to metaphase, in AB cells. In contrast to AB cells, in P_1 cells, after NEBD,
200 NPP-21-GFP reorganized around mitotic chromosomes in a metaphase plate to adopt a
201 structure that resembled the mitotic spindle, similar to a spindle matrix. In 25% of two cell
202 embryos, both AB and P_1 cells exhibited this spindle-like localization (Figure 2B). Thus, in P_1
203 cells 100% of the time, and in AB cells 25% of the time, NPP-21-GFP adopts a localization
204 pattern during mitosis that resembles the spindle matrix.
205
206 We have previously shown that some factors required for spindle checkpoint strength, such as
207 PCH-2-GFP, are enriched in P_1 cells (Defachelles et al., 2020). To determine whether NPP-21-
208 GFP is also enriched in P_1 cells, we quantified the average fluorescence of NPP-21-GFP that
209 remained around mitotic chromosomes in the timepoint immediately after NEBD (images
210 labeled 20 seconds in Figure 2B). We performed this quantification at this stage of the cell cycle
211 since this localization was similar in both AB and P_1 cells immediately after NEBD and entry into
212 mitosis, in contrast to the changes in localization we observed at metaphase in AB and P_1 cells
213 (Figure 2B). When we performed this analysis, we detected more NPP-21-GFP in P_1 cells than
214 AB cells (Figure 2C). We were concerned that, even at this early timepoint, the area occupied
215 by NPP-21-GFP was also different in AB and P_1 cells, potentially affecting this quantification. To
216 test this, we determined the area occupied by NPP-21-GFP signal in AB and P_1 cells and found
217 that this area was significantly smaller in P_1 cells than AB cells (Figure 2D). Since AB and P1
218 cells show similar nuclear areas prior to NEBD (Gerhold et al., 2018), this indicates that NPP-
219 21-GFP is regulated differently in P_1 cells even at this early timepoint. However, when we
220 calculated the integrated intensity of NPP-21-GFP signal (Figure 2E) in both cell types, NPP-21-
221 GFP signal was still significantly higher in P_1 cells than AB cells, indicating that NPP-21-GFP is
222 enriched in P_1 cells, potentially to drive the stronger checkpoint.

223

224 **NPP-21 concentrates PCH-2-GFP around mitotic chromosomes**

225

226 We showed that the stronger checkpoint in P_1 cells is controlled by the asymmetric enrichment
227 of the conserved ATP-ase, PCH-2, in P_1 cells (Defachelles et al., 2020). PCH-2 and its
228 mammalian ortholog, Trip13, remodels active Mad2 to generate inactive Mad2 (Ye et al., 2015).
229 This remodeling guarantees the availability of inactive Mad2 during checkpoint activation so that
230 the conversion of inactive Mad2 to active Mad2 is the rate limiting event in spindle checkpoint
231 activation (Ma and Poon, 2016; Ma and Poon, 2018; Nelson et al., 2015). Based on this activity,
232 we proposed that an increase in PCH-2 promotes the stronger checkpoint in P_1 cells by
233 increasing the amount of available, inactive Mad2 that could contribute to soluble MCC
234 formation and drive a stronger checkpoint response (Defachelles et al., 2020).

235

236 To evaluate whether NPP-21 contributed to the stronger spindle checkpoint in P_1 cells by
237 regulating PCH-2, we generated a strain that had both *AID::npp-21* and a tagged, functional
238 version of *pch-2*, *pch-2::GFP-3xFLAG* (Nelson et al., 2015). Both *npp-21* and *pch-2* are closely
239 linked (0.20 cM apart). To generate the *AID::npp-21 pch-2::GFP-3xFLAG* double mutant strain,
240 the TIR1 transgene, also on the same chromosome, was crossed off in the recombination event.
241 Since we observed the defect in checkpoint strength in P_1 cells even in embryos that have not
242 been treated with auxin (Figure 1D), we first determined whether we could perform this
243 experiment in worms that did not express the TIR1 transgene. These double mutants do not
244 exhibit any embryonic inviability, indicating that the embryonic inviability we observe in *AID-*
245 *3xFLAG::npp-21 Pgld-1::TIR1-mRuby* strains on ethanol was likely the product of inappropriate
246 TIR1 activity (Table 1). *AID-3xFLAG::npp-21 pch-2::GFP-3xFLAG* hermaphrodites did produce
247 males at a higher, statistically significant frequency than *pch-2::GFP-3xFLAG* animals,
248 suggesting a very weak defect in meiotic chromosome segregation (Table 1). However, *AID-*

249 *3xFLAG::npp-21 pch-2::GFP-3xFLAG* embryos display a stronger checkpoint in P_1 cells, similar
250 to control animals (Figure 3A), indicating that *AID-3xFlag::npp-21* is fully functional and the
251 weaker checkpoint we observed in *3xFLAG::npp-21 Pgld-1::TIR1-mRuby* P1 cells was a
252 product of the presence of the TIR1 gene.
253
254 We introduced *Psun-1::TIR1-mRuby* into strains with *AID-3xFLAG::npp-21 pch-2::GFP-*
255 *3xFLAG*. Strains carrying AID-NPP-21, this transgenic version of TIR1 and PCH-2-GFP showed
256 a weaker spindle checkpoint in P_1 cells, similar to AB cells and in contrast to control animals and
257 strains with only AID-NPP-21 and PCH-2-GFP (Figure 3A). This phenotype was also similar to
258 the original strain expressing only AID-NPP-21 and TIR1 (Figure 1D). When these worms were
259 grown on plates containing ethanol, we observed an increase in male self-progeny and no effect
260 on viability (Table 1).
261
262 We quantified PCH-2-GFP in both AB and P_1 cells in embryos expressing only AID-NPP-21 and
263 PCH-2-GFP (no TIR1) or expressing AID-NPP-21, TIR1 and PCH-2-GFP (Figures 3B and C).
264 Both strains with and without TIR1 showed statistically significant enrichment of PCH-2-GFP in
265 P_1 cells, compared to AB cells (Figure 3D). However, we noticed that the area occupied by
266 PCH-2-GFP increased in both AB and P_1 cells in strains expressing TIR1 (Figure 3E and
267 Supplemental Figure 1). Moreover, in P_1 cells without TIR1, the area occupied by PCH-2-GFP
268 was larger than that observed in AB cells without TIR1, likely because PCH-2-GFP often
269 adopted a matrix-like structure in P_1 cells (55%, 6 of 11 embryos) (Figure 3C and Supplemental
270 Figure 1). However, this structure was much less defined than the one observed with NPP-21-
271 GFP (Figure 2B). When the area occupied by PCH-2-GFP was used to calculate the integrated
272 density of PCH-2-GFP in AID-NPP-21 embryos with and without TIR1, P_1 cells in strains with
273 TIR1 were still enriched for PCH-2-GFP but the comparison with AB cells was not statistically
274 significant (Figure 3F). This was in direct contrast to the experiments performed in embryos with

275 no TIR1 (Figure 3F). These data indicate that NPP-21 is not required to enrich PCH-2-GFP in P_1
276 cells but instead, contributes to its concentration around mitotic chromosomes in both AB and P_1
277 cells. Given the defect in checkpoint strength in P_1 cells, we would argue that this concentration
278 is particularly important for the stronger checkpoint in P_1 cells. The inability to properly
279 concentrate PCH-2-GFP in P_1 cells may also explain why PCH-2-GFP rarely adopts a matrix-
280 like structure in P_1 cells in embryos expressing AID-NPP-21 and TIR1 (18%, 2 of 11 embryos)
281 (Figure 3C and Supplemental Figure 1).
282
283 **NPP-21 promotes GFP-MAD-2 recruitment to unattached kinetochores in P_1 cells**
284
285 In both *Drosophila* and in vitro cell cultured human (HeLa) cells, the NPP-21 ortholog, Megator
286 (*Drosophila*) and TPR (humans), contributes to Mad2, but not Mad1, localization to unattached
287 kinetochores (Lince-Faria et al., 2009; Schweizer et al., 2013). In *Drosophila*, Megator has been
288 proposed to act as a spatial regulator of Mad2 (Lince-Faria et al., 2009) while in human cells,
289 TPR appears to ensure the stability of checkpoint proteins for checkpoint function (Schweizer et
290 al., 2013). To test what effect NPP-21 had on Mad2 recruitment to unattached kinetochores
291 (Figures 4A and B), we quantified GFP-MAD-2 at unattached kinetochores in both AB and P_1
292 cells in *AID::npp-21* embryos, treated with either ethanol or auxin (Figures 4B and C). AB cells
293 in embryos treated with ethanol or auxin did not exhibit any difference in GFP-Mad2 recruitment
294 to unattached kinetochores (Figures 4B and C), consistent with the checkpoint activation we
295 observed in these cells (Figure 1C). GFP-Mad2 localization in P_1 cells treated with ethanol
296 resembled the AB cells we analyzed, indicating that the weaker spindle checkpoint in these cells
297 is not the result of a defect in Mad2 recruitment (Figures 4B and C). By contrast, in P_1 cells
298 treated with auxin, GFP-Mad2 localization to unattached kinetochores was sharply reduced
299 (Figures 4B and C), demonstrating that the weaker checkpoint response in these cells was

300 explained by the inability to robustly localize Mad2 to unattached kinetochores, similar to what
301 has been reported in *Drosophila* and HeLa cells.
302
303 During early development, embryos balance the rapid cell divisions of early embryogenesis with
304 the imperative of maintaining genomic integrity, particularly in immortal germline tissue that will
305 give rise to sperm and eggs. NPP-21, through its spindle matrix function, contributes to this
306 balance by promoting a stronger spindle checkpoint response in germline cells, in contrast to
307 somatic cells. The NPP-21 protein displays germline specific behavior: it is enriched and
308 consistently forms a spindle matrix in P_1 cells, suggesting a conserved developmental role
309 during embryogenesis. This function acts at two control points: concentrating PCH-2 around
310 mitotic chromosomes and promoting Mad2 recruitment to unattached kinetochores. Given PCH-
311 2's role in promoting the availability of inactive, open Mad2 for checkpoint signaling, it's formally
312 possible that these two control points are mechanistically linked. Whether other, conserved
313 spindle matrix components play similar, developmental, roles during embryogenesis is an
314 interesting, open question for our future studies.
315
316 **Materials and Methods**
317
318 ***C. elegans* Strains and Husbandry**
319 The wildtype *C. elegans* strain background was Bristol N2 (Brenner, 1974) . All strains were
320 maintained at 20°C. See Supplemental Table 1 for a list of all *C. elegans* strains used in this
321 study.
322
323 The AID::3xFLAG::NPP-21 transgenic strain was generated by CRISPR/Cas9 genomic editing
324 (Paix et al., 2017). Young adult worms carrying the *Pgld-1::Tir1mRuby::3'UTR(gld-1) (ieSi64)*
325 transgene were injected with preassembled Cas9-RNP, 23 ng/µL of ssDNA repair template and

326 5 ng/uL pCFJ90 and 2.5 ng/uL pCFJ104 as co-injection markers. The target crRNA was
327 TAGTCTTTCAGTTATGGATG (IDT) and the ssDNA repair template was generated by primer
328 extension PCR using the following primer
329 GTGTTATCTAATTAAATCTCTCAGTTCCTTCAAGTTATCATAT and gBlock
330 CTCTCAGTTCCTTCAAGTTATCATATTTTTTAAGTAAAACTAATCGCCCGAAATTTAGTCTTTCA
331 GTTATGCCTAAAGATCCAGCCAAACCTCCGGCCAAGGCACAAGTTGTGGGATGGCCACCG
332 GTGAGATCATACCGGAAGAACGTGATGGTTTCCTGCCAAAAATCAAGCGGTGGCCCGGAG
333 GCGGCGGCGTTCGTGAAGGACTATAAAGATCACGACGGAGATTACAAGGACCATGATATCG
334 ACTACAAGGACGACGACGACAAGGGAGATGTGGATGCGCCACTTCAGGCGCCTGAACAAC
335 CGGTCGCAGACGCTGACGATGAAGAAGCTAACTGGGAAATGGAAAAAGCCGAAATGAAAC
336 GGATTGAG (both ordered from IDT). Transformants were identified and worms carrying the
337 transgene were genotyped using the following primers: AATTGGCATCGCTGATCAATGAG and
338 GCTCTTTAATTTCAGCCGCATGAC. The presence of the transgene was verified by
339 sequencing and the transgenic strain was backcrossed at least three time before analysis.
340

341 **Viability and fertility**

342 To score total progeny and male self-progeny, L4 hermaphrodites were picked onto individual
343 plates with auxin, ethanol or no additional treatment, and transferred to new plates daily over 4
344 days. The eggs laid on each plate were counted after removing the parent. Viable progeny and
345 male progeny were quantified when the F1 reached L4 or adult stages (2-3 days post egg
346 laying).
347

348 **Microscopy & Mitotic Timing Experiments**

349 All immunofluorescence and live microscopy was performed on a DeltaVision Personal DV
350 deconvolution microscope (Applied Precision) equipped with a 100X N.A. 1.40 oil-immersion
351 objective (Olympus) coupled with a CoolSNAP charge-coupled camera (Roper Scientific). For

352 live microscopy of two cell embryos, eggs were dissected 18-26 hours post-L4 into 1X Egg
353 Buffer (25mM Hepes pH7.4, 118uM NaCl, 48mM KCl, 2mM EDTA, 0.5mM EGTA) and mounted
354 on 2% agarose pads for immediate analysis. Environmental temperature averaged 21°C during
355 image collection for all experiments. For mitotic timing experiments, Z-sections were acquired
356 with 8x 2µm steps using a 100X objective (Olympus) at 20s intervals. Exposure time was 100ms
357 for mCherry-H2B and 50ms for GFP-PH. Mitotic duration was calculated for the AB cell in the
358 presence of monopolar spindles as the interval between NEBD to the onset of cortical
359 contractility (OCC) or the interval between NEBD and chromosome decondensation (DECON).
360 NEBD was defined by the equilibration of mCherry-H2B from the nucleus into the cytosol. OCC
361 was defined as the change in conformation of the plasma membrane from circular to
362 rectangular, or with *zyg-1* RNAi as the first frame when a persistent membrane bleb formed from
363 the cortex of the embryo. DECON was defined as the loss of punctate mCherry-H2B signal
364 within the decondensing chromatin. To minimize bleaching and maximize signal intensity of
365 GFP-tagged spindle checkpoint components (NPP-21, PCH-2 and MAD-2), imaging was started
366 just after NEBD as visualized by mCherry-H2B. Here, 8x 1µm steps were captured with 250ms
367 GFP and 100ms mCherry exposures at 20s intervals.
368
369 Immunostaining was performed on worms 20–24 h after L4 stage, as described in (Russo et al.,
370 2021). Gonad dissections were performed in 1× EBT (250 mM Hepes-Cl, pH 7.4, 1.18 M NaCl,
371 480 mM KCl, 20 mM EDTA, and 5 mM EGTA) + 0.1% Tween 20 and 20 mM sodium azide. An
372 equal volume of 7.4% formaldehyde in EBT (final concentration was 3.7% formaldehyde) was
373 added and allowed to incubate under a coverslip for 5 min. The sample was mounted on
374 HistoBond slides (75 × 25 × 1 mm from Lamb), freeze-cracked, and incubated in methanol at
375 −20°C for slightly more than 1 min and transferred to PBST (PBS with Tween 20). After several
376 washes of PBST, the samples were incubated for 30 min in 1% bovine serum albumin diluted in
377 PBST. A hand-cut paraffin square was used to cover the tissue with 50 µl of antibody solution.

378 Incubation was conducted in a humid chamber overnight at 4°C. Slides were rinsed in PBST
379 and then incubated for 2 h at room temperature with fluorophore-conjugated secondary antibody
380 at a dilution of 1:500. Samples were rinsed several times and DAPI stained in PBST, then
381 mounted in 13 µl of mounting media (20 M *N*-propyl gallate [Sigma-Aldrich] and 0.14 M Tris in
382 glycerol) with a no. 1 1/2 (22 mm^2) coverslip, and sealed with nail polish.
383
384 Mouse anti-FLAG [Sigma] primary antibodies were used for immunofluorescence at 1:1000 and
385 Alexa-Fluor 488 anti-mouse (Invitrogen) secondary antibodies were used at 1:500. Three-
386 dimensional image stacks were collected at 0.2-µm Z-spacing and processed by constrained,
387 iterative deconvolution. Image scaling and analysis were performed using functions in the
388 softWoRx software package. Projections were calculated by a maximum intensity algorithm.
389 Composite images were assembled and some false coloring was performed with Adobe
390 Photoshop.
391
392 **Quantification of NPP-21-GFP, GFP-MAD-2, and PCH-2-GFP-3XFLAG**
393 Analysis was performed in Fiji. Quantification of fluorescence around mitotic chromosomes was
394 quantified as described in (Defachelles et al., 2020). Sum intensity projections were generated
395 and average fluorescence in the area around mitotic chromosomes was measured in Fiji.
396 Background average fluorescence was measured in a 30-pixel band around this “cloud” and
397 subtracted from the initial fluorescence intensity to determine the final value. In some of our
398 movies to quantify PCH-2-GFP and localize NPP-21-GFP, identifying a clear metaphase plate
399 was more difficult in AB than in P1 cells. Therefore, to ensure that we were performing these
400 experiments at the same stage in mitosis in these two cell types, frames for the relevant
401 analysis were normalized relative to NEBD and mitotic exit.
402

403 Quantification of unattached kinetochore signal was performed essentially as described for
404 GFP-MAD-2 quantification in (Nelson et al., 2015). Maximum intensity projections of both
405 mCherry-H2B and GFP fusion proteins were made after the pseudo-metaphase plate was
406 generated. The image was rotated so the metaphase plate was vertical, channels were split,
407 and the maximum GFP pixel was identified using the process function within a box on the
408 unattached side of the metaphase plate. In the same x-plane, the maximum mCherry-H2B pixel
409 was found. The width was changed to 12 pixels and the maximum GFP signal intensity was
410 recorded in this 12 pixel window centered at the mCherry maxima. The background GFP signal
411 was calculated by taking the average GFP intensity of a 4 pixel box in the same x-plane, 8
412 pixels away from the maximum mCherry on the opposite side of the pseudo-metaphase plate to
413 the maximum GFP (i.e. the attached side). This background GFP was then subtracted from the
414 maximum to measure the kinetochore bound GFP fusion intensity. This process was repeated at
415 least 7x for each genetic background and treatment.
416
417 **Feeding RNA interference (RNAi)**
418 RNA interference (RNAi) was performed by growing relevant worm strains on HT115 bacteria
419 transformed with a vector allowing for IPTG inducible expression of dsRNA against the *zyg-1*
420 gene. Bacterial strains containing this RNAi vector were cultured overnight at 37°C, centrifuged,
421 and the pellet was re-suspended in 1/10 of the original volume. 50uL of concentrated culture
422 was spotted onto a nematode growth medium (NGM) plate with 1mM IPTG and 50ug/uL of
423 kanamycin and the RNAi spot was allowed to grow overnight at 37°C. Plates were stored at 4°C
424 for up to 10 days.
425
426 L4 hermaphrodite worms were transferred to RNAi plates, allowed to incubate for 2–3 hours,
427 and then transferred to fresh RNAi plates. Live microscopy was performed on embryos 22–26

428 hours after worms were picked to the *zyg-1* RNAi plate. HT115 bacteria transformed with
429 pHSG298 (Clontech) was used as a control for *zyg-1*^{RNAi}.
430
431 **Auxin treatment**
432 Auxin treatment was performed on worms 20–24 hours after L4 stage by transferring worms to
433 bacteria-seeded plates containing auxin or ethanol. The natural auxin indole-3-acetic acid (IAA)
434 was purchased from Alfa Aesar (#A10556). A 100 mM stock solution in ethanol was prepared
435 and was stored at 4°C for up to two months. 100ul of the auxin stock solution or ethanol was
436 added to NGM plates (volume 10mls) to achieve a final concentration of 1mM.
437
438 To perform RNAi against *zyg-1* and auxin treatment, L4 hermaphrodite worms were transferred
439 to RNAi plates, allowed to incubate for 2–3 hours, and then transferred to fresh RNAi plates for
440 20-22 hours. Worms were then transferred to RNAi plates containing either auxin or ethanol to
441 incubate for 2-3 hours before performing live microscopy.
442
443 **Statistical Analysis**
444 Data was analyzed using Prism for statistical significance. For Figures 2C, D and E, student's t-
445 test was used to assess significance. For all other data, one-way ANOVA with Šídák correction
446 was used to assess significance.
447
448 **Acknowledgements**
449 We would like to thank Arshad Desai, Karen Oegema, Peter Askjaer and Geraldine Seydoux for
450 valuable *C. elegans* strains. We thank the members of the Bhalla lab for reading of the
451 manuscript. This work and the resulting manuscript was supported by the National Institutes of
452 Health (NIH) (grant numbers R35GM141835 [N.B.], T32GM133391 [S.B.] and R01GM065591
453 [A.F.D.]), a postdoctoral fellowship of the Human Frontier Science Program (LT000903/2013-C

454 [S.K.]) and the Howard Hughes Medical Institute (A.F.D.). Some strains were provided by the
455 CGC, which is funded by NIH Office of Research Infrastructure Programs (P40 OD010440).
456
457 Because this manuscript is the result of funding in whole or in part by the NIH, this manuscript is
458 subject to the NIH Public Access Policy. Through acceptance of this federal funding, NIH has
459 been given a right to make this manuscript publicly available in PubMed Central upon the
460 Official Date of Publication.
461
462

463 **References**

464

465 Baker, D.J., K.B. Jeganathan, J.D. Cameron, M. Thompson, S. Juneja, A. Kopecka, R. Kumar,
466 R.B. Jenkins, P.C. de Groen, P. Roche, and J.M. van Deursen. 2004. BubR1
467 insufficiency causes early onset of aging-associated phenotypes and infertility in mice.
468 *Nat Genet*. 36:744-749.

469 Brenner, S. 1974. The genetics of Caenorhabditis elegans. *Genetics*. 77:71-94.

470 Cohen-Fix, O., and P. Askjaer. 2017. Cell Biology of the Caenorhabditis elegans Nucleus.
471 *Genetics*. 205:25-59.

472 Collin, P., O. Nashchekina, R. Walker, and J. Pines. 2013. The spindle assembly checkpoint
473 works like a rheostat rather than a toggle switch. *Nat Cell Biol*. 15:1378-1385.

474 Defachelles, L., A.E. Russo, C.R. Nelson, and N. Bhalla. 2020. The conserved AAA-ATPase
475 PCH-2 (TRIP13) regulates spindle checkpoint strength. *Mol Biol Cell*. 31:2219-2233.

476 Essex, A., A. Dammermann, L. Lewellyn, K. Oegema, and A. Desai. 2009. Systematic analysis
477 in Caenorhabditis elegans reveals that the spindle checkpoint is composed of two largely
478 independent branches. *Mol Biol Cell*. 20:1252-1267.

479 Galli, M., and D.O. Morgan. 2016. Cell Size Determines the Strength of the Spindle Assembly
480 Checkpoint during Embryonic Development. *Dev Cell*. 36:344-352.

481 Gerhold, A.R., V. Poupart, J.C. Labbe, and P.S. Maddox. 2018. Spindle assembly checkpoint
482 strength is linked to cell fate in the Caenorhabditis elegans embryo. *Mol Biol Cell*.
483 29:1435-1448.

484 Huang, L., W. Li, X. Dai, S. Zhao, B. Xu, F. Wang, R.T. Jin, L. Luo, L. Wu, X. Jiang, Y. Cheng, J.
485 Zou, C. Xu, X. Tong, H.Y. Fan, H. Zhao, and J. Bao. 2023. Biallelic variants in
486 MAD2L1BP (p31(comet)) cause female infertility characterized by oocyte maturation
487 arrest. *Elife*. 12.

488 Kops, G.J., B.A. Weaver, and D.W. Cleveland. 2005. On the road to cancer: aneuploidy and the
489 mitotic checkpoint. *Nat Rev Cancer*. 5:773-785.
490 Kyogoku, H., and T.S. Kitajima. 2017. Large Cytoplasm Is Linked to the Error-Prone Nature of
491 Oocytes. *Dev Cell*. 41:287-298 e284.
492 Lara-Gonzalez, P., J. Pines, and A. Desai. 2021. Spindle assembly checkpoint activation and
493 silencing at kinetochores. *Semin Cell Dev Biol*. 117:86-98.
494 Lince-Faria, M., S. Maffini, B. Orr, Y. Ding, F. Claudia, C.E. Sunkel, A. Tavares, J. Johansen,
495 K.M. Johansen, and H. Maiato. 2009. Spatiotemporal control of mitosis by the conserved
496 spindle matrix protein Megator. *J Cell Biol*. 184:647-657.
497 Ma, H.T., and R.Y. Poon. 2016. TRIP13 Regulates Both the Activation and Inactivation of the
498 Spindle-Assembly Checkpoint. *Cell Rep*. 14:1086-1099.
499 Ma, H.T., and R.Y.C. Poon. 2018. TRIP13 Functions in the Establishment of the Spindle
500 Assembly Checkpoint by Replenishing O-MAD2. *Cell Rep*. 22:1439-1450.
501 Matthews, H.K., C. Bertoli, and R.A.M. de Bruin. 2022. Cell cycle control in cancer. *Nat Rev Mol*
502 *Cell Biol*. 23:74-88.
503 Nelson, C.R., T. Hwang, P.H. Chen, and N. Bhalla. 2015. TRIP13PCH-2 promotes Mad2
504 localization to unattached kinetochores in the spindle checkpoint response. *J Cell Biol*.
505 211:503-516.
506 O'Connell, K.F., C. Caron, K.R. Kopish, D.D. Hurd, K.J. Kemphues, Y. Li, and J.G. White. 2001.
507 The C. elegans zyg-1 gene encodes a regulator of centrosome duplication with distinct
508 maternal and paternal roles in the embryo. *Cell*. 105:547-558.
509 Paix, A., A. Folkmann, and G. Seydoux. 2017. Precision genome editing using CRISPR-Cas9
510 and linear repair templates in C. elegans. *Methods*. 121-122:86-93.
511 Qi, H., U. Rath, D. Wang, Y.Z. Xu, Y. Ding, W. Zhang, M.J. Blacketer, M.R. Paddy, J. Girton, J.
512 Johansen, and K.M. Johansen. 2004. Megator, an essential coiled-coil protein that

513 localizes to the putative spindle matrix during mitosis in Drosophila. *Mol Biol Cell*.
514 15:4854-4865.
515 Robertson, S., and R. Lin. 2013. The oocyte-to-embryo transition. *Adv Exp Med Biol*. 757:351-
516 372.
517 Russo, A.E., C.R. Nelson, and N. Bhalla. 2021. Mutating two putative phosphorylation sites on
518 ZHP-3 does not affect its localization or function during meiotic chromosome
519 segregation. *MicroPubl Biol*. 2021.
520 Schweizer, N., C. Ferras, D.M. Kern, E. Logarinho, I.M. Cheeseman, and H. Maiato. 2013.
521 Spindle assembly checkpoint robustness requires Tpr-mediated regulation of
522 Mad1/Mad2 proteostasis. *J Cell Biol*. 203:883-893.
523 Thomas, L., B. Taleb Ismail, P. Askjaer, and G. Seydoux. 2023. Nucleoporin foci are stress-
524 sensitive condensates dispensable for C. elegans nuclear pore assembly. *EMBO J*.
525 42:e112987.
526 Ye, Q., S.C. Rosenberg, A. Moeller, J.A. Speir, T.Y. Su, and K.D. Corbett. 2015. TRIP13 is a
527 protein-remodeling AAA+ ATPase that catalyzes MAD2 conformation switching. *eLife*. 4.
528 Zhang, L., J.D. Ward, Z. Cheng, and A.F. Dernburg. 2015. The auxin-inducible degradation
529 (AID) system enables versatile conditional protein depletion in C. elegans. *Development*.
530 142:4374-4384.
531 Zhang, Z., B. Li, J. Fu, R. Li, F. Diao, C. Li, B. Chen, J. Du, Z. Zhou, J. Mu, Z. Yan, L. Wu, S. Liu,
532 W. Wang, L. Zhao, J. Dong, L. He, X. Liang, Y. Kuang, X. Sun, Q. Sang, and L. Wang.
533 2020. Bi-allelic Missense Pathogenic Variants in TRIP13 Cause Female Infertility
534 Characterized by Oocyte Maturation Arrest. *Am J Hum Genet*. 107:15-23.
535 Zheng, Y. 2010. A membranous spindle matrix orchestrates cell division. *Nat Rev Mol Cell Biol*.
536 11:529-535.
537
538

539 **Table 1: Viability of strains**

540

541 **Figure Legends**

542

543 **Figure 1: NPP-21 is required for the stronger spindle checkpoint in germline cells of the**
544 **two-cell embryo.** A. AID-3xFLAG-NPP-21 is degraded in oocytes after one hour of auxin
545 treatment. Images of cellularized (-1) oocytes from worms treated with ethanol or auxin stained
546 with antibodies against the FLAG tag and DAPI to visualize DNA. Scale bar indicates 5 microns.
547 B. Cartoon indicating a two cell embryo with the AB and P_1 cell labeled and the nucleus colored
548 magenta. C. AID-3XFLAG-NPP-21 is functional and not required for the spindle checkpoint in
549 AB, somatic, cells. Graph depicting mitotic timing in AB cells of embryos treated with ethanol or
550 auxin and control RNAi or *zyg-1* RNAi. D. AID-3XFLAG-NPP-21 cannot support the stronger
551 checkpoint and is required for a robust spindle checkpoint in P_1, germline, cells. Graph
552 depicting mitotic timing in P_1 cells of embryos treated with ethanol or auxin and control RNAi or
553 *zyg-1* RNAi. A **** indicates a p value < 0.0001, a * indicates a p value < 0.05 and all error bars
554 indicate 95% confidence intervals.

555

556 **Figure 2: NPP-21-GFP is enriched in P_1, germline, cells and its localization is distinct**
557 **from that in AB, somatic, cells.** A. NPP-21-GFP is functional for the spindle checkpoint in AB
558 and P_1 cells. A graph depicting mitotic timing in AB and P_1 cells of control and *npp-21::GFP*
559 animals treated with control and *zyg-1* RNAi. B. NPP-21-GFP localization in P_1 cells is different
560 than in AB cells in most two cell embryos. Images of AB and P_1 cells expressing mCherry-H2B
561 (magenta) and NPP-21-GFP (green) at NEBD, 20 seconds after NEBD and at metaphase (120
562 seconds after NEBD). C. GFP-NPP-21 is asymmetrically enriched in P_1 cells. Graph depicting
563 average fluorescence of NPP-21-GFP in AB and P_1 cells 20 seconds after NEBD. D. The area
564 occupied by GFP-NPP-21 is smaller in P_1 cells. Graph depicting the area in microns^2 of NPP-

565 21-GFP in AB and P_1 cells 20 seconds after NEBD. E. GFP-NPP-21 is asymmetrically enriched
566 in P_1 cells. Graph depicting integrated intensity of NPP-21-GFP in AB and P_1 cells 20 seconds
567 after NEBD. A **** indicates a p value < 0.0001, a *** indicates a p value < 0.001, a * indicates a
568 p value < 0.05 and all error bars indicate 95% confidence intervals.
569
570 **Figure 3: NPP-21 concentrates PCH-2-GFP around mitotic chromosomes in both AB and**
571 **P_1 cells.** A. Worms expressing both AID-3XFLAG-NPP-21 and TIR1 cannot support the
572 stronger checkpoint. A graph depicting mitotic timing in AB and P_1 cells of control, *AID::npp-21*
573 and *AID::npp-21;TIR1* animals treated with control and *zyg-1* RNAi. B. Cartoon of PCH-2-GFP
574 localization in AB and P_1 cells. C. Images of PCH-2-GFP (green) localization in AB and P_1 cells
575 expressing mCherry-H2B (magenta) in metaphase, in embryos without and with the TIR1 gene.
576 Scale bar indicates 5 microns. D. PCH-2-GFP is asymmetrically enriched in P_1 cells, in embryos
577 without and with the TIR1 gene. Graph depicting average fluorescence of PCH-2-GFP in AB and
578 P_1 cells at metaphase. E. The area occupied by PCH-2-GFP is greater in AB and P_1 cells in
579 embryos expressing TIR1. Graph depicting the area in microns^2 of PCH-2-GFP in AB and P_1
580 cells in metaphase. E. PCH-2-GFP is less concentrated in P_1 cells of embryos expressing TIR1.
581 Graph depicting integrated intensity of PCH-2-GFP in AB and P_1 cells. A * indicates a p value <
582 0.05 and all error bars indicate 95% confidence intervals.
583
584 **Figure 4: NPP-21 is required for GFP-MAD-2 recruitment to unattached kinetochores in**
585 **P_1, germline, cells.** A. Cartoon of GFP-MAD-2 localization in AB and P_1 cells in *zyg-1*^{RNAi}
586 embryos. B. Images of GFP-MAD-2 (green) localization in AB and P_1 cells in *zyg-1*^{RNAi} embryos
587 expressing mCherry-H2B (magenta), treated with ethanol (top) or auxin (bottom). Scale bar
588 indicates 5 microns. C. Quantification of GFP-MAD-2 in AB and P_1 cells at unattached
589 kinetochores in *zyg-1*^{RNAi} embryos treated with ethanol or auxin. A *** indicates a p value <
590 0.001 and all error bars indicate 95% confidence intervals.

591

592 **Supplemental Figure 1: Grayscale images of PCH-2-GFP in *AID::npp-21* strains without**

593 **(top) and with TIR1 (bottom).** Area of enrichment indicated by yellow dotted circle. Scale bar

594 indicates 5 microns.

595

596 **Supplemental Table 1: *C. elegans* strains used in this study**

597

Table 1: Viability of strains

Genotype and condition	Embryonic viability (number of embryos)	% Males
Control + ethanol	100% (2165)	0.05%
Control + auxin	100% (1799)	0.08%
AID-3xFLAG::npp-21 Pgld-1::TIR-1-mRuby + ethanol	96% (2245)****	2.3%****
AID-3xFLAG::npp-21 Pgld-1::TIR-1-mRuby + auxin	0.25% (1598)****	25%****
pch-2::GFP-3xFLAG	100% (3061)	0.06%
AID-3xFLAG::npp-21 pch-2::GFP-3xFLAG	100% (3373)	0.6%***
AID-3xFLAG::npp-21 Psun-1::TIR-1-mRuby	100% (2113)	1.7%****

A *** indicates a P value < 0.001 and a **** indicates a P value < 0.0001

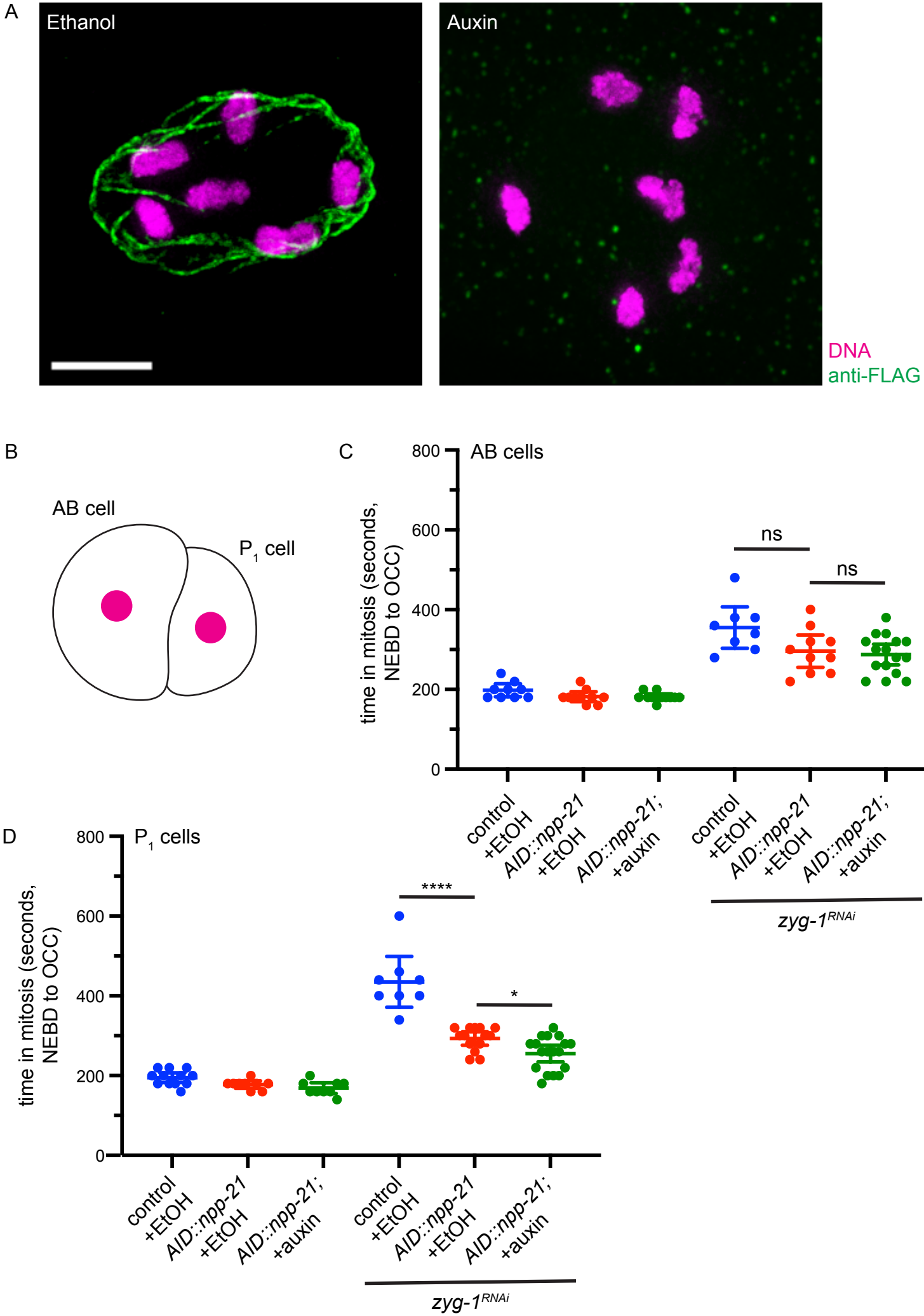
A
Ethanol
Auxin
DNA
anti-FLAG
B
AB cell
P1 cell
C
AB cells
time in mitosis (seconds, NEBD to OCC)
800
600
400
200
0
ns
ns
control +EtOH
AID::npp-21 +EtOH
AID::npp-21; +auxin
control +EtOH
AID::npp-21 +EtOH
AID::npp-21; +auxin
zyg-1RNAi
D
P1 cells
time in mitosis (seconds, NEBD to OCC)
800
600
400
200
0
****
*
control +EtOH
AID::npp-21 +EtOH
AID::npp-21; +auxin
control +EtOH
AID::npp-21 +EtOH
AID::npp-21; +auxin
zyg-1RNAi

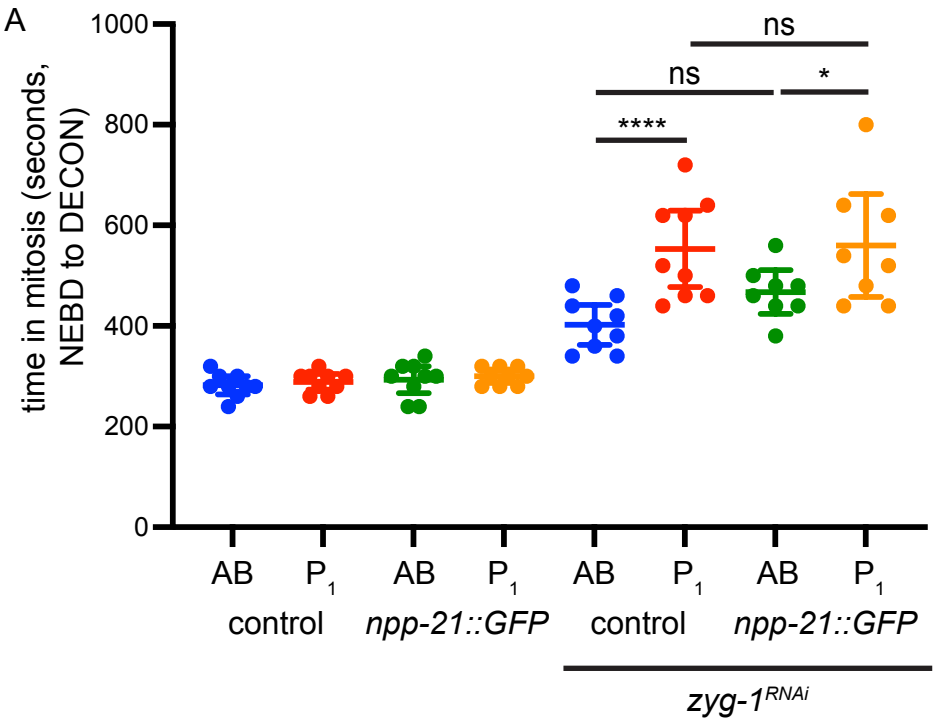
A
time in mitosis (seconds, NEBD to DECON)
1000
800
600
400
200
0
ns
ns
*
****
AB
P1
AB
P1
AB
P1
AB
P1
control
npp-21::GFP
control
npp-21::GFP
zyg-1RNAi

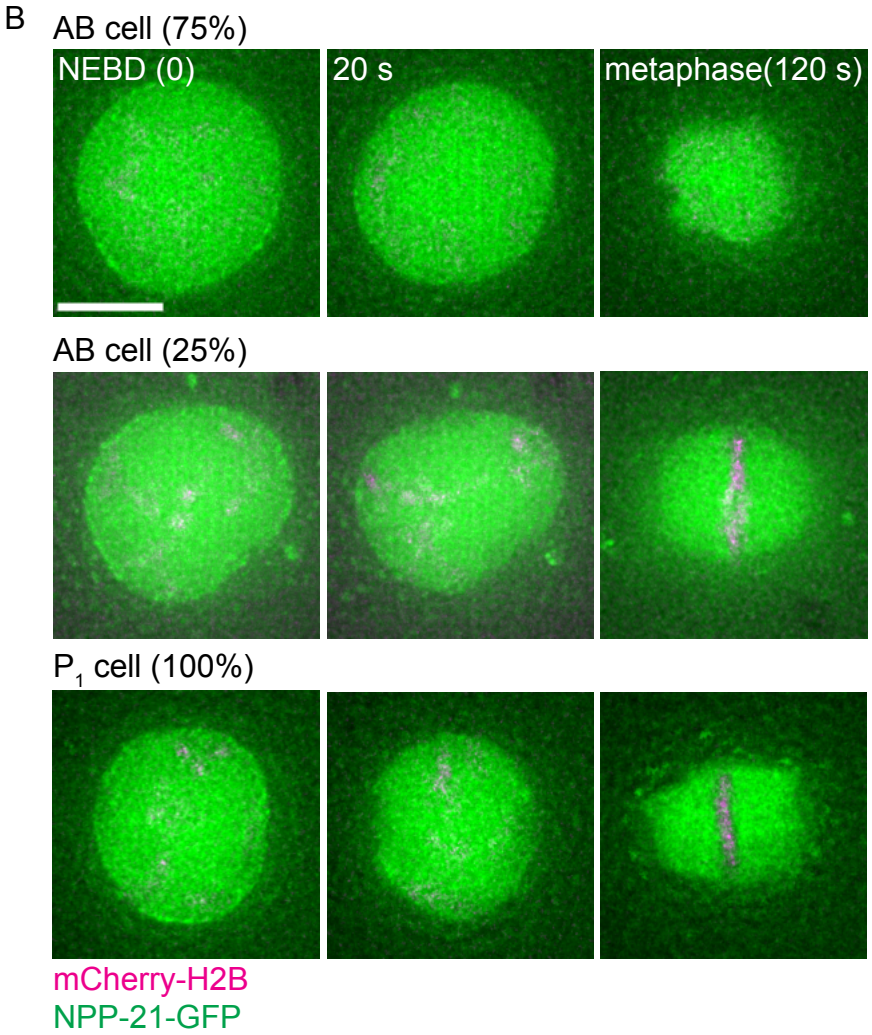
B
AB cell (75%)
NEBD (0)
20 s
metaphase(120 s)
AB cell (25%)
P1 cell (100%)
mCherry-H2B
NPP-21-GFP

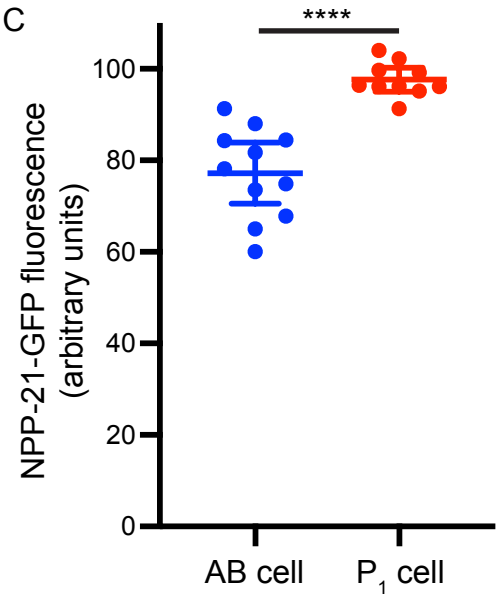
C
NPP-21-GFP fluorescence (arbitrary units)
100
80
60
40
20
0
****
AB cell
P1 cell

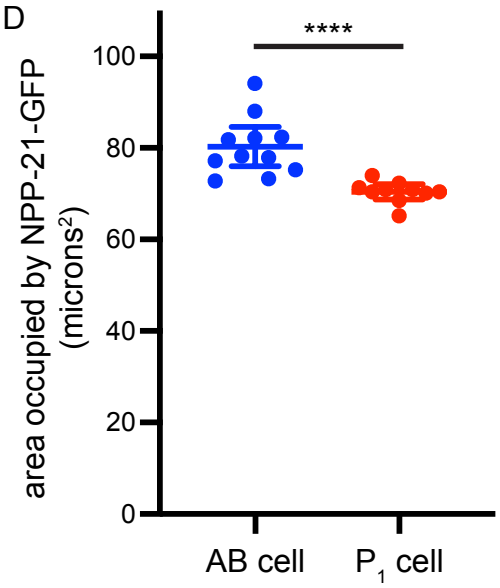
D
area occupied by NPP-21-GFP (microns2)
100
80
60
40
20
0
****
AB cell
P1 cell

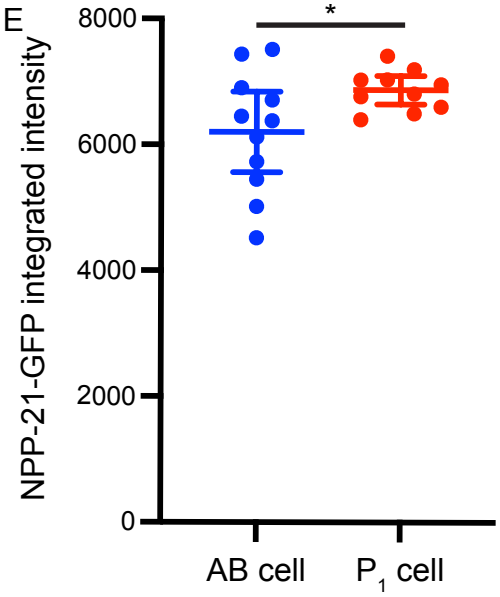
E
NPP-21-GFP integrated intensity
8000
6000
4000
2000
0
*
AB cell
P1 cell

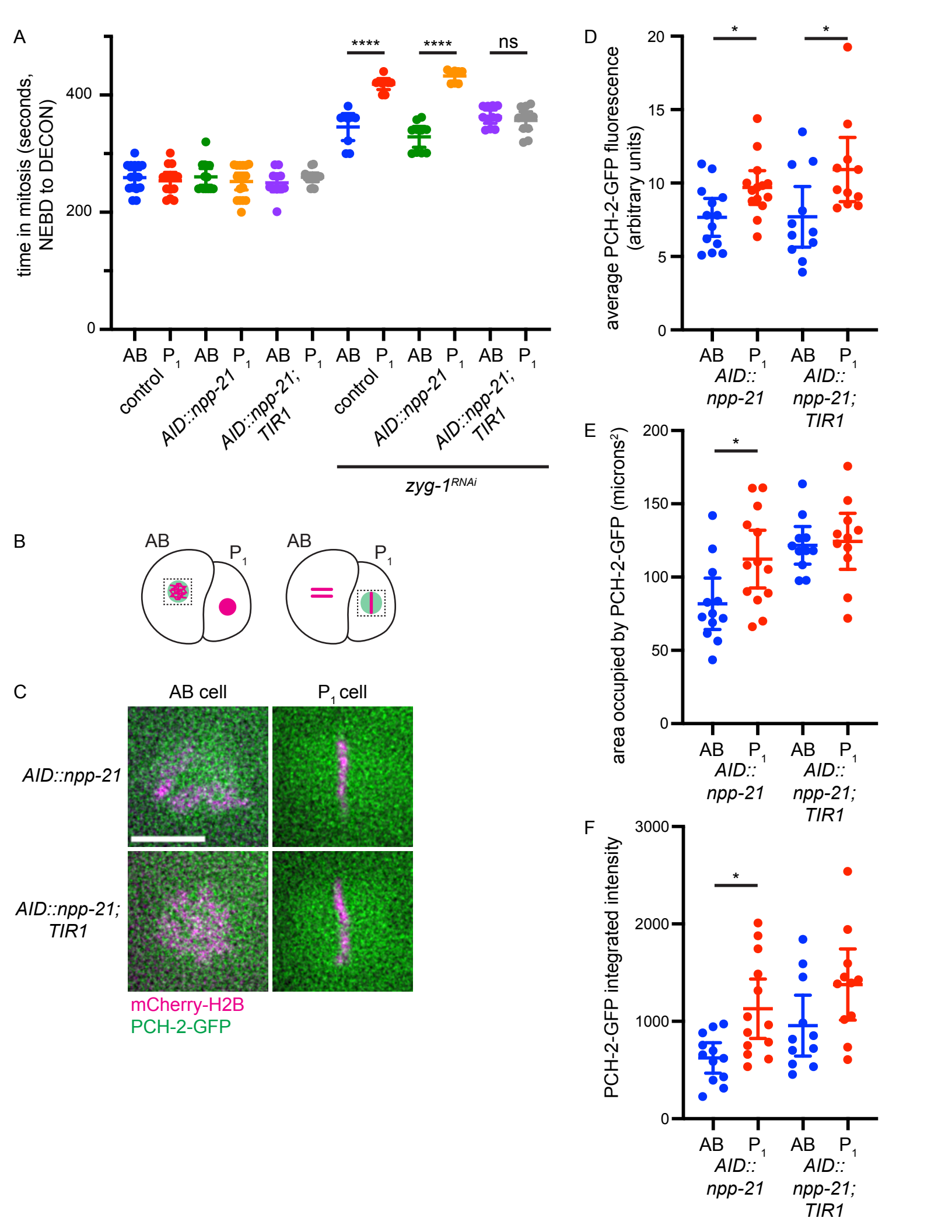
A
time in mitosis (seconds, NEBD to DECON)
0
200
400
****
****
ns
AB
P1
control
AID::npp-21
AID::npp-21; TIR1
zyg-1RNAi
B
AB
P1
C
AB cell
P1 cell
AID::npp-21
AID::npp-21; TIR1
mCherry-H2B
PCH-2-GFP
D
average PCH-2-GFP fluorescence (arbitrary units)
0
5
10
15
20
*
*
AID:: npp-21
AID:: npp-21; TIR1
E
area occupied by PCH-2-GFP (microns2)
0
50
100
150
200
*
F
PCH-2-GFP integrated intensity
0
1000
2000
3000
*

A

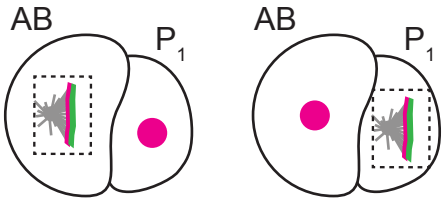
AB
P1
AB
P1

B

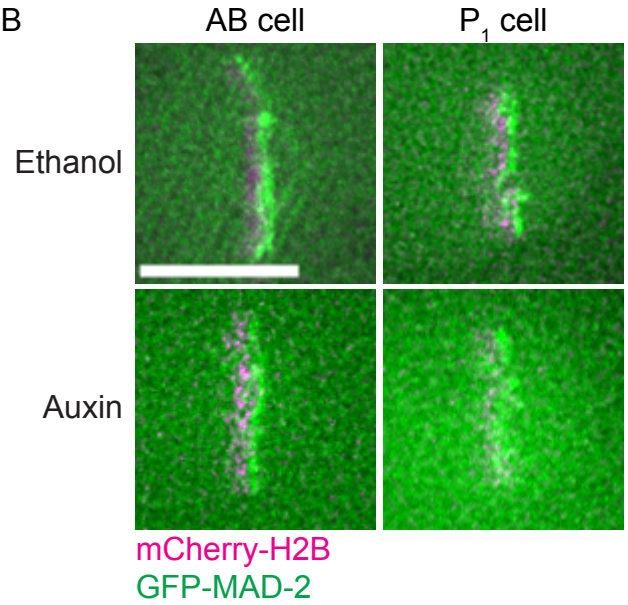
AB cell
P1 cell
Ethanol
Auxin
mCherry-H2B
GFP-MAD-2

C

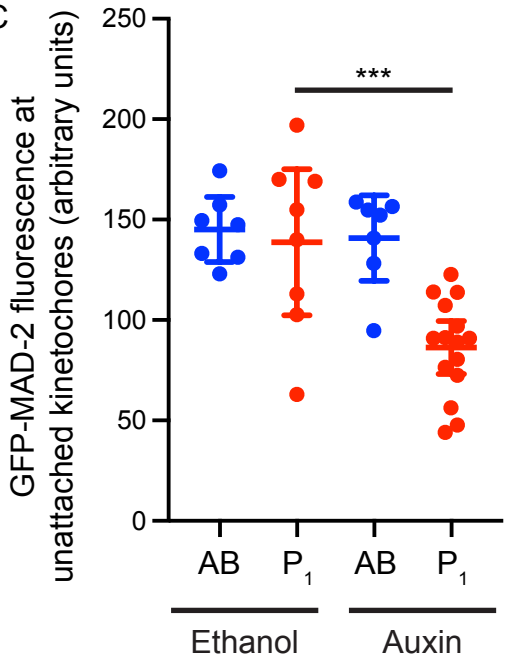
GFP-MAD-2 fluorescence at unattached kinetochores (arbitrary units)
250
200
150
100
50
0
***
AB
P1
AB
P1
Ethanol
Auxin